



RESEARCH ARTICLE

10.1029/2022JD037956

Key Points:

- A general-purpose Monte-Carlo model of gamma-ray glow production is presented
- Plausible Gamma-ray Glow production conditions are provided for five previous airborne observations
- Some cases could be explained by the Modification of Spectrum mechanism only while other require electric fields close to Relativistic Runaway Electron Avalanche process threshold, or above

Correspondence to:

D. Sarria,
david.sarria@uib.no

Citation:

Sarria, D., Østgaard, N., Marisaldi, M., Lehtinen, N., & Mezentsev, A. (2023). Library of simulated gamma-ray glows and application to previous airborne observations. *Journal of Geophysical Research: Atmospheres*, 128, e2022JD037956. <https://doi.org/10.1029/2022JD037956>

Received 30 SEP 2022

Accepted 18 APR 2023

Author Contributions:

- Conceptualization:** D. Sarria, N. Østgaard, M. Marisaldi
Data curation: D. Sarria
Formal analysis: D. Sarria
Funding acquisition: N. Østgaard, M. Marisaldi
Investigation: D. Sarria, N. Østgaard, A. Mezentsev
Methodology: D. Sarria, N. Østgaard, M. Marisaldi
Project Administration: N. Østgaard, M. Marisaldi
Resources: D. Sarria
Software: D. Sarria
Supervision: D. Sarria, N. Østgaard, M. Marisaldi
Validation: D. Sarria, N. Østgaard, A. Mezentsev
Visualization: D. Sarria

© 2023. The Authors.

This is an open access article under the terms of the Creative Commons Attribution License, which permits use, distribution and reproduction in any medium, provided the original work is properly cited.

Library of Simulated Gamma-Ray Glows and Application to Previous Airborne Observations

D. Sarria¹ , N. Østgaard¹ , M. Marisaldi^{1,2} , N. Lehtinen¹, and A. Mezentsev¹ 

¹Birkeland Centre for Space Science, University of Bergen, Bergen, Norway. ²INAF-OAS Bologna, Bologna, Italy

Abstract Gamma-Ray Glows (GRGs) are high energy radiation originating from thunderclouds, in the MeV energy regime, with typical duration of seconds to minutes, and sources extended over several to tens of square kilometers. GRGs have been observed from detectors placed on ground, inside aircraft and on balloons. In this paper, we present a general purpose Monte-Carlo model of GRG production and propagation. This model is first compared to a model from Zhou et al. (2016, <https://doi.org/10.1016/j.astropartphys.2016.08.004>) relying on another Monte-Carlo framework, and small differences are observed. We then have built an extensive simulation library, made available to the community. This library is used to reproduce five previous gamma-ray glow observations, from five airborne campaigns: balloons from Eack et al. (1996b, <https://doi.org/10.1029/96gl02570>), Eack et al. (2000, <https://doi.org/10.1029/1999gl010849>); and aircrafts from ADELE (Kelley et al., 2015, <https://doi.org/10.1038/ncomms8845>), ILDAS (Kochkin et al., 2017, <https://doi.org/10.1002/2017jd027405>) and ALOFT (Østgaard et al., 2019, <https://doi.org/10.1029/2019jd030312>). Our simulation results confirm that fluxes of cosmic-ray secondary particles present in the background at a given altitude can be enhanced by several percent (MOS process), and up to several orders of magnitude (RREA process) due to the effect of thunderstorms' electric fields, and explain the five observations. While some GRG could be explained purely by the MOS process, E-fields significantly larger than E_{th} are required to explain the strongest GRGs observed. Some of the observations also came with in-situ electric field measurements, that were always lower than E_{th} , but may not have been obtained from regions where the glows are produced. This study supports the claim that kilometer-scale E-fields magnitudes of at least the level of E_{th} must be present inside some thunderstorms.

Plain Language Summary Gamma-Ray Glows (GRGs) are high-energy radiation that originates from thunderclouds. These radiations fall within the MeV energy range and last for seconds to minutes. The sources of GRGs are typically extended over a few to tens of square kilometers. In this study, we developed a general-purpose model to understand the production of GRGs, including the cosmic ray fluxes and enhancement by thunderstorm's electric field, propagation, and instrumental response. Using this model, we were able to reproduce and constrain five previously reported airborne GRG observations, two from balloons, and three from aircraft. The results of our study showed that all of the observations could be explained by one of the two expected regimes: one involving purely particle acceleration (MOS: Modification of Spectrum) and the other involving particle multiplication (RREA: Relativistic Runaway Electron Avalanche). Our simulations suggest that the required large-scale thunderstorm electric fields, which are compatible with our results, are generally larger than what was previously measured.

1. Introduction

Gamma-Ray Glows (GRGs) are high energy photon radiation originating from thunderclouds, with a typical time-scale of a second to minutes, and can extend over an area of tens of squared kilometers, that is, the scale of thunderclouds. GRGs can also be referred as Thunderstorm Ground Enhancements (TGE) by some authors, but we choose to keep the former terminology for the rest of this article because we are focusing on airborne observations. A review of the GRG observations and other high energy atmospheric physics phenomena is provided in Dwyer et al. (2012). GRGs have been observed from detectors placed on ground (typically 0–4 km altitude), aircrafts and balloons (typically 4–20 km altitude). Ground observations of GRG were reported in Torii et al. (2009), Brunetti et al. (2000), Chubenko et al. (2000), Torii et al. (2002), Tsuchiya et al. (2007), Wada et al. (2018, 2021) (and references therein), sometimes associated with neutrons, electrons and positron signatures (Babich, 2003; Chilingarian et al., 2010, 2012, 2013; Enoto et al., 2017; Gurevich et al., 2012; Tsuchiya et al., 2012). Several aircraft-based observations of GRG were reported by Parks et al. (1981), McCarthy and

Writing – original draft: D. Sarria, N. Østgaard, M. Marisaldi, A. Mezentsev
Writing – review & editing: D. Sarria

Parks (1985), Kelley et al. (2015), Kochkin et al. (2017), Østgaard et al. (2019) (see also references therein). Several balloon-based observations of GRG were reported by (Eack et al., 1996a, 1996b, 2000). Eack and Beasley (2015) conducted simulations of several GRGs observed from three balloon flights in 1995. The glows were measured at altitudes between 4 and 8 km, and they used analytical modeling to estimate the electric field inside the thunderstorm in order to reproduce the increase in glow flux. They found that all of the GRG events required an electric field above the break-even field, which is equal to $E_{be} = 216$ kV/m at sea level and scales with air density. In this article, we put the focus on higher altitude events. A GRG was also observed preceding a Terrestrial Gamma-ray Flash and it is proposed that they could be a necessary requirement for TGF production, as they can induce enough amplification of a Relativistic Runaway Electron Avalanche (Smith et al., 2018; Wada et al., 2019). When a leader is developed in a region that already has the electric field above E_{th} , the leader field will add to it and potentially create conditions to produce a TGF.

The detected photon spectrum of a GRG is consistent with bremsstrahlung radiation from high energy electrons. Following the original idea of Wilson (1925), electrons can run away, that is, get continuously accelerated by electric fields present in thunderclouds, as the field acceleration overcomes the friction force from the air. It requires appropriate electron energy ε and electric field magnitude E . Following the idea of Gurevich et al. (1992), the electron population can further grow by the effect of collisions knocking out other electrons from the medium. This results in a Relativistic Runaway Electron Avalanche (RREA), that is also referred as runaway breakdown in the literature. RREA triggers with different probabilities for different (ε, E) values, and an evaluation of this probability distribution is presented in Chanrion et al. (2016), Lehtinen (2000), Sarria et al. (2018), using several models and methods. To be initiated, the RREA process requires electrons above a given energy threshold ε_c (that are called “seed electrons”) and an electric field above a threshold, the “RREA threshold” of $E_{th} = 284$ kV/m at sea level (scales proportionally with air density). In the case of GRGs, these seeds come from the background radiation, that is, cosmic ray secondaries (extensive air showers). In addition to the RREA process, a Relativistic Feedback effect (RF) can contribute significantly to the electron multiplication if the electric field is increased further above E_{th} . The RF mechanism consists of the possibility for positrons and back-scattering x-rays to come back inside the avalanche region and consequently induce the production of more RREAs, that will increase the electron multiplication factor even more. In other words, there will be an “avalanche” of RREAs. The state of the feedback process is parameterized by a γ factor, that gives the rate at which the RREAs are multiplied. It has three states:

- If $\gamma \ll 1$, it just provides a small enhancement of the electron multiplication.
- If γ is large enough, but <1 , it can increase the electron multiplication factor by several orders of magnitude, and reach a steady-state where relativistic electrons are continuously generated over a long period of time, until an external factor breaks it.
- If $\gamma > 1$, the system becomes limited by the number of RREAs that increases exponentially, and produce a macroscopic number of electrons (theoretically infinitely), which produces a current flow that will discharge (partially or fully) the electric-field region. That is to say, the RREA space charge becomes significant enough to affect the external field (Dwyer, 2012).

Zhou et al. (2016), Bartoli et al. (2018) quantified the variations of both electron and positron background fluxes reaching a detector located at 4.3 km altitude, as a function of the electric field of the thundercloud above the detector. The E-field is vertical with upward values in the -100 kV/m to $+100$ kV/m range (about $\pm 0.6E_{th}$). It was modeled for a specific geometrical configuration, in order to reproduce observations of background enhancements observed during thunderstorms by the ARGO-YBJ cosmic ray detector, located in Tibet. Since the involved electric fields are about 40% below the RREA threshold (i.e., there is no, or marginal electron multiplication), the underlying mechanism explaining this flux increase (resp. decrease; depending on the sign of the field) is that the charged particles gain (resp. lose) kinetic energy from the thunderstorm’s electric field, and travel longer (resp. shorter) distances in the air. Therefore more (resp. fewer) background particles are able to reach the detector, compared to fair weather conditions. This effect is usually called the “Modification of the Spectrum” (MOS) mechanism (Chilingarian et al., 2010). Zhou et al. (2016) shows, with in their geometrical configuration using an electric field set between 4.3 and 6.3 km altitude and using a low energy threshold of 100 keV, that the electron number flux could increase by a factor of 2.2 for an electric field of -100 kV/m, while the positron content could increase by a factor of 1.8 for an electric field of $+100$ kV/m. However, it is also worth noting that the high energy photon content only increases by a factor of about 1.2 and 1.1 for -100 kV/m and $+100$ kV/m respectively. This

is because high energy photons already make up 92% of the background content, with electrons typically accounting for only 6% and positrons for only 2%.

In Section 2, we describe our Monte-Carlo model to simulate the enhancement of cosmic ray secondary photons, electrons and positrons by thunderstorms' electric fields. In Section 3, we apply this model to independently reproduce the simulation results presented by Zhou et al. (2016) at mountain altitude and with electric fields below the RREA threshold, and discuss how the two models compare. In Section 4, we present the results of our model, when it is extended from 10 to 20 km (aircraft and balloon altitudes), and to electric fields above the RREA threshold, in order to simulate several previous airborne gamma-ray glow observations. We discuss the results in Section 5, and we conclude in Section 6.

2. Monte-Carlo Model Description

We have developed a computer model able to simulate and record the effect of thunderstorm electric fields on the fluxes of cosmic ray secondary particles. The code and final data products are made freely available on a public online repository, see the Open Research section. Our approach assumes that the glow is not evolving with time and has a fixed intensity for a given fixed parameter set (the parameters of the models are described below). Our model uses the GEANT4 toolkit (Agostinelli et al., 2003; Allison et al., 2006), version 10.07, that is freely available. We used the O4 physics list for electro-magnetic processes (with careful check of the stepping process, see Sarria et al. (2018)), the high precision Bertini cascade model for the hadronic processes, and the default GEANT4 processes for the other physics. Our model is coupled with the PARMA code (also freely available, see the Open Research section) that gives us the distributions of cosmic ray secondaries: energy, altitude, and zenith angle, of photons, electrons, positrons, neutrons and protons (Sato, 2016; Sato et al., 2008). The cosmic ray particles can be sampled at a discrete altitude, or inside a given altitude range. We also integrated the NRLMSISE-00 model to simulate the atmosphere between 0 and 25 km altitude. GEANT4 is a powerful modular Monte-Carlo simulation toolkit developed by the European Organization for Nuclear Research (CERN) in association with a worldwide collaboration. It is used to simulate particle propagation through matter with or without electro-magnetic fields. The ability of GEANT4 to simulate particle propagation in the context of thunderstorms and high-energy atmospheric radiation was extensively tested against several custom models used by the high-energy atmospheric physics community (Rutjes et al., 2016; Sarria et al., 2018; Skeltved et al., 2014).

PARMA gives estimates of the cosmic-ray spectra of neutrons, protons, muons, electrons, positrons, photons and ions (helium and heavier). It is based on empirical analytical formulas fitted on the results of runs of the Monte-Carlo code PHITS (Sato et al., 2008). The later requires quite large resources to run, and PARMA was produced to make it possible to rapidly compute cosmic radiation doses with a precision equivalent to that of PHITS. The accuracy of the data provided by PARMA was verified against different sets of experimental data, taken under various conditions, in a large range of altitudes (Sato et al., 2018). Later versions of the software extended its validity to higher altitudes and added angular distributions for the particles.

Figure 1 illustrates the geometrical configuration of our simulation. The parameters of the model are:

- H_E : the altitude of the center of the electric field region.
- ΔH_E : the full (vertical) size of the electric field region, that is, E is between $H_E - \Delta H_E/2$ and $H_E + \Delta H_E/2$.
- H_D : the altitude of particle detection (record).
- ΔU : the total potential difference applied on the electric field region. Positive ΔU means downward E , that is, electrons are accelerated upward.

The density varies along this geometry according to the profile given by the NRLMSISE-00 model. The Electric field remains constant within its region, therefore the strength of the electric field relatively to the RREA threshold (i.e., E/E_{th}) varies with altitude. The simulation uses an electric field area (X-Y plane) of significantly larger than the recorded X-Y plane area, ensuring that a detection made in the center is not impacted by border effects, as verified through careful examination.

In some of the configurations we are using, the electric field may be either in the MOS regime, or larger than the RREA threshold E_{th} . When the RREA threshold is reached and exceeded, the Relativistic Feedback (RF) effect will increase its significance as the electric field and so the feedback factor γ increases. We expect 3 simulation states, purely driven by the high energy Monte-Carlo simulation, that is, not accounting for disturbances in the

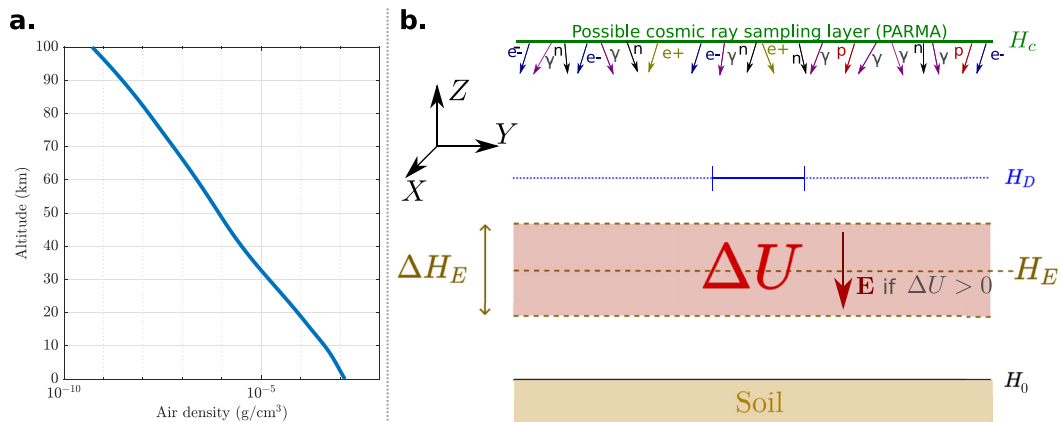


Figure 1. (a) Altitude as function of atmospheric density given by the NRLMSISE-00 model. (b) Geometrical configuration of the simulation based on the GEANT4, PARMA and NRLMSISE-00 codes. Initial cosmic rays are generated by the PARMA code at altitude H_C , the particle tracking is done with GEANT4, and the atmospheric densities are obtained from NRLMSISE-00. The electric field layer (in red) is centered at altitude H_E , and has a size ΔH_E that contains a potential difference ΔU (Positive ΔU means electrons accelerated upwards). The detection layer is located at altitude H_D , and is positioned above the electric field region for illustration, but can be set at any altitude between 0 and 25 km. The cosmic-ray sampling layer, represented in green, can also be positioned at any altitude. The (initial) sampled particle energy range is 40 keV–900 GeV, and the record range is 25 keV–100 MeV (before applying the case-by-case instrumental response).

charge structure of the thundercloud that could be due to the production of large amounts of charged particles. The 3 states are:

- (i) MOS dominated: the E-field $E < E_{\text{th}}$, gives an increase of path length and energies of electrons (or positrons for opposite field polarity) that increases their amounts locally and makes electrons (or positrons) produce more Bremsstrahlung radiation (but there is no significant multiplication). The expected photon fluence increase in this case is about several percent to about 20% above background.
- (ii) RREA dominated: $E \gtrsim E_{\text{th}}$, exponential increase of electrons as function of time. The multiplication of particles is dominated by the RREA process, and the increase due to the MOS effect only becomes negligible. Some level of feedback is also possible but does not dominate the multiplication (i.e., there can be some positrons or x-rays scattering backwards in the electric field region and producing extra electrons multiplication). This regime is able to produce photon flux increases from a factor 10 to about several 1000 s above background (this is before absorption that happens between the production region and the detector).
- (iii) Feedback dominated: $E > E_{\text{th}}$. In this case $\gamma > 1$ and the particle increase is expected to be able to reach 10^6 or more. This produces an exponential increase and can be maintained for unlimited time in the simulation (not taking into account space charges). Kelley et al. (2015) indicates a feedback threshold in the context of GRG production of 400 kV/m at sea level, that is 1.4 times E_{th} . Note that for significant feedback to occur, one must also satisfy requirements on the volume occupied by the field (Dwyer, 2012). For this study we fixed a maximum time limit of about 6 avalanche times (estimated from previous knowledge of avalanche rates for given uniform field E). This regime was not properly explored in this study because it produces computational problems with our approach, and another approach, time-driven, is needed (see Skeltved et al. (2014) for an implementation of such approach in air at sea level).

First, a cut-off energy of $\varepsilon_c = 100$ keV was set (this means that particles with lower energies are discarded), similar to what is used by Zhou et al. (2016), whose model is compared to our own in the next section. In our simulation, we employed a lower threshold for the electron kinetic energy, $\varepsilon_c = 8$ keV. This value represents a conservative lower limit of the minimum energy required for RREA to occur in an electric field at the very large critical field magnitude, $E_c = 26$ MV/m (or 26,000 kV/m) at sea level (Sarria et al., 2018). Tracking particles with energy below this threshold would not affect the outcome of the simulation. With electric fields lower than the RREA threshold (i.e., the case for the comparison we present in Section 3) both 8 and 100 keV energy thresholds were tested, and presented similar results. However, when the simulation is extended to E-fields above the RREA threshold, it can produce a significant change in the results, as any electrons above $\varepsilon_c = 8$ keV is a potential seed for the RREA process (Sarria et al., 2018). The value of ε_c is actually dependent on the E-field magnitude, but

rather than using a variable value, it was easier for us to use a single, conservative, lower limit for ε_c of 8 keV for all our simulations.

3. Comparison to Previous Modeling

The first step of this study was to compare our model with results from previous modeling effort presented in Zhou et al. (2016) and Bartoli et al. (2018). They quantified, for the first time (to our knowledge), the variations of both electron and positron background fluxes reaching a detector, as function of the electric field of the thundercloud, located on top of the detector, this last being located on a mountain at 4.3 km altitude. They used a different modeling strategy than us. Their method is fully based on the CORSIKA code, and starts by sampling high energy cosmic protons at high altitude, to calculate the distribution of secondary particles by comprehensively simulating the particle showers in the atmosphere. In our model, this part was pre-calculated by the PARMA based on the PHITS code (see previous section), and we start from lower altitude sources of photons, electrons, positrons, neutrons and protons, and the tracking and interactions of particles is processed by GEANT4. We use the definition that a positive potential difference ΔU implies a positive electric field pointing downwards, and therefore electrons accelerated upwards.

The configuration used by Zhou et al. (2016) for studying the ARGO-YBJ detector results, can be reproduced by our model by setting $H_E = 5.3$ km, $\Delta H_E = 2$ km, $H_D = 4.3$ km. They applied an electric field from $-1,000$ kV/m to $1,000$ kV/m ($=100$ kV/m), that is equivalent in our modeling by setting a potential ΔU between -200 and $+200$ MV inside the E-field layer, which is about 60% of the RREA threshold for $H_E = 5.3$ km.

Figure 2 shows the variation fluxes of electrons and positrons as function of the applied electric field obtained by Zhou et al. (2016), compared to our model. The bottom panel shows the relative difference in electron and positron fluxes between the two models.

We can first discuss the flux variations of electrons and positrons. For positive (resp. negative) electric fields, the electrons (resp. positrons) traveling in the direction of the detector are decelerated, therefore the detected number of particles is decreasing, down to about -20% for $E = +100$ kV/m (resp. $E = -100$ kV/m). In this case, the two models show a very good agreement with less than 5% differences. For negative (resp. positive) electric fields, the electrons (resp. positrons) traveling in the direction of the detector are accelerated. Therefore the detected number of particles is increasing, up to about 100% for positrons when $E = +100$ kV/m, and up to 140% for electrons when $E = -100$ kV/m. The two models show a very good agreement (less than 5% difference) for $|E| < 60$ kV/m. For larger $|E|$ the models show a larger discrepancy: the difference goes up to 20% for positrons at $E = +100$ kV/m, and goes up to about 33% for electrons when $E = -100$ kV/m; our model presenting systematically larger variations.

These differences cannot be attributed to an effect of the cut-off energy ε_c , as we tested both 100 and 8 keV for our model, that lead to similar results. However this low energy limit is expected to be more significant for larger electric fields, at which the minimum runaway electron energy drops below the simulation cut-off energy (see Section 4). It is still unclear to us how the above differences between the two models could be explained. It is important to note that both models were independently constructed (one based on GEANT4 and the other on CORSIKA), with key potential differences being the physics implementation, including the cross-sections for both electro-magnetic and hadronic processes, the atmospheric models, and the particle propagation in the E-fields for precise particle tracking and records. We think both models are valid within the uncertainties of their respective building elements. Therefore, any discrepancies in the results should be interpreted as an estimate of the level of uncertainty resulting from the cumulative effect of all the small variations in the building elements.

It is worth noting that our Geant4-based model allows for adjustments to the stepping parameters of electrons in the electric field, such as artificially increasing the step size, in order to reduce electron energy gain and multiplication and align with the results of Zhou et al. (2016). However, it should be noted that our primary goal is to achieve the most accurate simulations possible based on our current understanding, rather than replicating their simulation results.

In addition of the electron and positron fluxes, our model also provides the variation of photons fluxes, presented in Figure 2 (black dots), that was not provided by Zhou et al. (2016). The increases are up to 20% for a $E = -100$ kV/m and up to 10% for $E = +100$ kV/m. In practice, these photons are more important than electrons

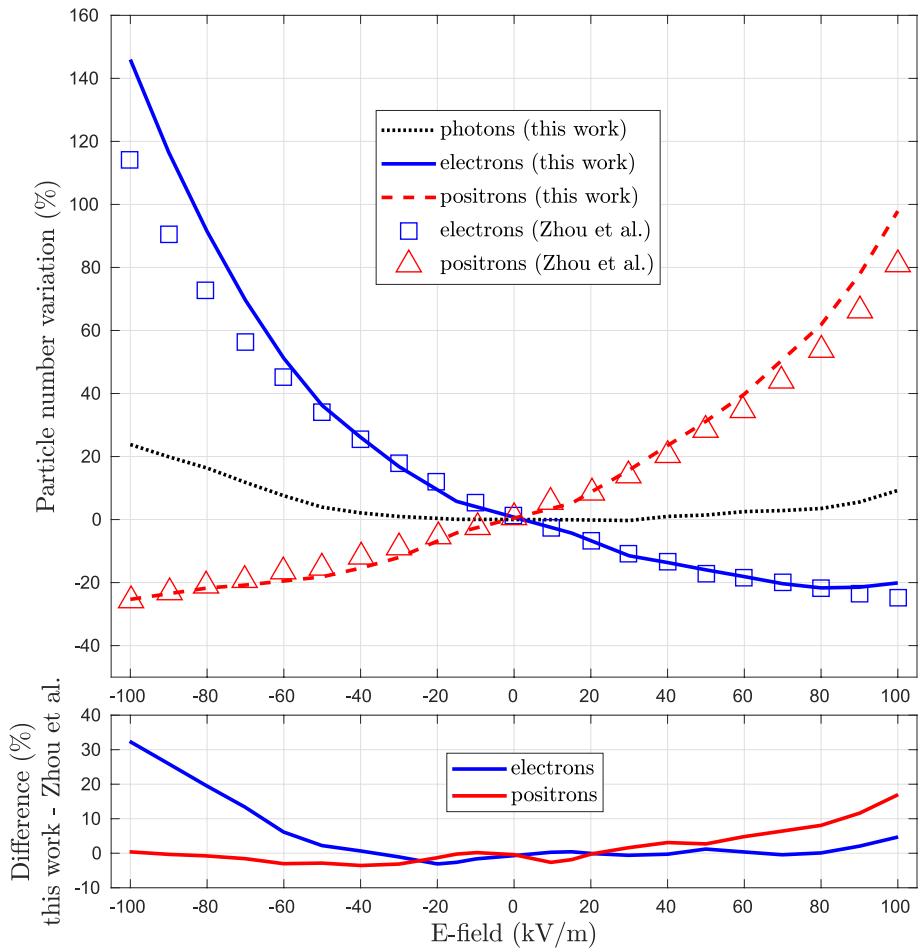


Figure 2. Top panel: fluxes of photons, electrons and positrons at 4.3 km altitude, as function of the applied electric field (E), relatively to the case where no electric-field is present (i.e., background). The maximum electric field tested here, of ± 100 kV/m, corresponds to about 60% of the RREA threshold. The electric field is located between 4.3 and 6.3 km altitude. The results of the model developed for this study are compared with previous results extracted from Zhou et al. (2016). The bottom panel is the relative difference between the two models, for electrons and positrons. Photon flux variations are also shown.

as they will propagate much larger distances and are expected to produce the main contribution on GRG when they are detected by instruments that could be located several kilometers away.

4. Application to Previous Gamma-Ray Glow (GRG) Airborne Observations

4.1. Simulation of GRGs and Instruments

Using the model described in Section 2, we built a library of GRG simulations. It is meant to be used for a large set of observational contexts (ground, aircraft, balloon). This library is made publicly available, see the data availability section. The library covers a wide range of parameters:

- The center of the electric field region located between $H_E = 4$ km and $H_E = 16$ km altitude. The used altitude grid is [4,6,8,10,12,14,15,16] (in km)
- Different values of ΔU so that the magnitude of the electric field is tested from 0 to 220 MV, with both polarities. The used potential grid is [$\pm 220, \pm 210, \pm 175, \pm 150, \pm 120, \pm 80, \pm 50, \pm 40, \pm 30, \pm 20, \pm 10, 0$] (in MV).
- An extension of the E-field region fixed to $\Delta H_E = 2$ km (full length). We could not test other E-field region lengths because of limited computation time/power availability.
- For each case, the particles are recorded in a set of distances from the center of the electric field region, as a multiplication factor m of $\Delta H_E/2$, so that the detection altitude is $H_D = H_E + m\Delta H_E/2$. ($\Delta H_E/2$ is always equal

to 1 km in this work). Values of m tested are $[0, -1, 1, -2, 2, -3, 3, -4, 4, -5, 5, -6, 6, -7, 7, -8, 8]$, but any H_D value below 4 km or above 20 km was not considered.

Figure 3 shows a simulation result to illustrate what is contained in the simulation library. In this case, the E-field center altitude H_E is set to 14 km and all the particles are recorded at $H_D = 15$ km altitude. Figure 3a shows the multiplication factors of photons, electrons and positrons as function of the applied potential. In this case the photons can increase by a factor of 260 (compared to background) when the potential reaches the largest tested value of 220 MV (i.e., above the RREA threshold of about 125 MV at this altitude) and a factor of 14 with a potential of -220 MV. At a potential of +125 MV, corresponding to the RREA threshold, the photon background is increased by a factor ≈ 1.7 , the electrons by a factor ≈ 16 , and the positrons are actually reduced by $\approx 20\%$ compared to background (multiplication factor of 0.80), as the electric field make them gain momentum downwards, away from the detector.

In Figure 3a, for positive potentials (electrons accelerated upwards), the number of recorded electrons is first due to the MOS mechanism (when $E < E_{th}$) and then to the RREA process (when $E > E_{th}$). Note that a change in the slope of the blue curve is observed around E_{th} : this is all the more important since the figure shows the variation in the number of particles on a logarithmic scale. The photon number follows the increase of electrons due to the bremsstrahlung process. The increase of the number of positron is due to the pair production mechanism by these created bremsstrahlung (energetic) photons.

In Figure 3a, for negative potentials (positrons accelerated upwards), the observed increase of recorded positron number is mostly due to the MOS process on background positrons (increased kinetic energy and path length). The observed increase of photons is due to bremsstrahlung by the enhanced positrons. The new photons can produce Compton electrons, and electron-positron pairs by pair production, that explain the observed increases.

Figures 3b–3g show, respectively, the photon, electron and positron spectra for different tested potentials between -220 and +220 MV. The absolute scale of the background spectrum for our model, in the absence of an electric field, can be obtained using PARMA. We have verified that our Monte-Carlo model is consistent with PARMA at lower altitudes. For Figure 3, the reference point at altitude $H_D = 15$ km provided by PARMA is $2.35 \text{ cm}^{-2} \cdot \text{s}^{-1} \cdot \text{MeV}^{-1}$ for a background (i.e., when $\Delta U = 0$) photon energy of 1.13 MeV. This reference point, allows to determine the absolute flux for any scenario with an electric field, as consistent relative values are always provided.

When the potential are increased from 0 to 220 MV, the photon and electron energy spectra evolve toward a characteristic RREA spectrum, namely power laws with an exponential cut-off. The number of positrons is increased due to pair production by high energy photons. These extra positrons have a different, softer, spectrum compared to background positrons, which are produced by a very different population of energetic photons.

When the potential is negative, from -220 to 0 MV, meaning that the electric field is pointing upwards, RREA is produced downwards and only the back-scattered RREA photons and their secondaries are detected. This implies the following for large negative potential (≤ -190 MV): 1. a harder photon spectrum, that is, with less pronounced RREA cut-off 2. a similar electron spectrum, but with a lower intensity for the same absolute value of potential 3. a positron spectrum much harder, as positrons have gained energy with the electric field but cannot produce more positrons (unlike electrons) and, like electrons, produce energetic electrons by inelastic scattering (also referred as Møller scattering in the literature). To be used at a later stage, these values of particle variations should be weighted with their amounts in the background: generally about 92% photon, 6% electrons and 2% positrons, which changes with altitude.

The measured enhancements above background presented above are also heavily affected by the characteristics of the instruments detecting them (actually, the final recorded particles are photons for most of the simulated cases). To be able to compare these simulation results to real data, the response of the considered instrument must also be taken into account. In this study we investigated five different observation made with four very different detectors. For ILDAS and ALOFT missions, the mass models of the instruments (plus environment) were built closely with the relevant teams during previous studies (Kochkin et al., 2018; Østgaard et al., 2019). For the balloon observations of Eack et al., an approximative GEANT4-based model as been built by us for this study, using information provided in Eack (1996), Eack et al. (1996a, 1996b, 2000). The GEANT4-based geometrical model takes into account 5 cm diameter by 2 mm thick NaI scintillation crystal with a 1 mm thick aluminum entrance window, the detector window foam insulation (2.5 cm), the outer shield, a crude model of the PMT, the helium balloon, the sonde and the electric field meter. In Eack (1996) the NaI crystal is sensitive from 30

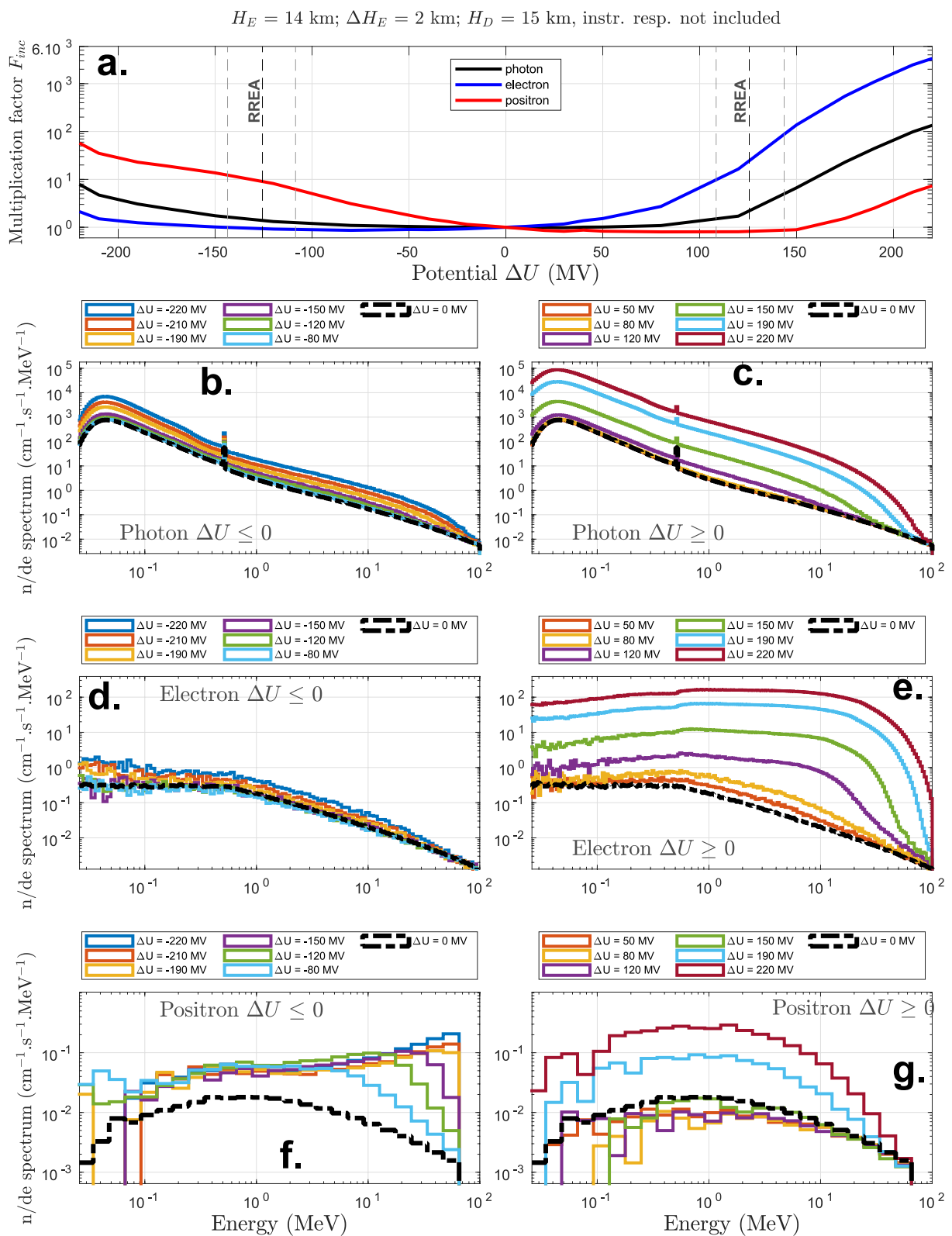


Figure 3.

Table 1

Main Parameters of the Five Gamma-Ray Glow Observations That Were Simulated

Campaign	Detector energy range, MeV	Effective area, cm ²	Altitude, km	Flux increase factor F_{inc}	Surrounding material
Eack-1996 ^a	0.03–0.12	78	15	3–50	Light ^b
Eack-2000 ^c	0.06–0.3	156	14	1.6–3	Light ^b
ADELE ^d	0.05–5	161.3	14–15	1.2–10	Heavy ^e
ILDAS ^f	0.1–10	23	12	3–20	Heavy ^g
ALOFT ^h	0.3–30	225	20	1.2–1.45	Heavy ⁱ

^aEack et al. (1996b). ^bfoam close to NaI crystal, electronics, shielding, covering, balloon and electric field meters (far way). ^cEack et al. (2000). ^dKelley et al. (2015). ^eGulfstream-V aircraft. ^fKochkin et al. (2017). ^gA340 aircraft. ^hØstgaard et al. (2019). ⁱER-2 aircraft.

to 120 keV. It is important to understand that this corresponds to deposited energy into the crystal, but an incident photon with larger energies can also be detected. Eack et al. (2000) uses essentially the same gamma-ray spectrometer but with a thicker NaI crystal that increases the sensitivity range to 60–300 keV (NaI crystal thickness of 12.5 mm; private communication). A mass model of the ADELE instrument (and surrounding material) was provided by D.M. Smith (private communication), including an approximate model of the Gulfstream-V jet aircraft, upper/lower NaI and Plastic scintillators, and the lead shielding in-between. Note that for the ADELE campaign, only the plastic scintillators detected the GRGs since the NaI detectors operated in trigger mode and did not trigger for GRG observations (but triggered for TGF observations).

Table 1 summarizes the five observations that were simulated, including the detector energy range, the geometrical area of the detectors, and the amount of material surrounding the detector, the altitude of the observation, the observed range of the GRG maximum increase above background, and the associated reference paper. Each of the five campaigns' associated papers

reported several GRG observation. Table 1 also indicates the amount of material around each detector: it is very important in the simulation to take that into account, at least approximately. Indeed, more material means: (a) more absorption of the x/gamma-rays. (b) More interactions for the energetic electrons and positrons (above several MeV) therefore producing more bremsstrahlung radiation. (c) More positrons being stopped therefore more 511 keV photons being produced by positron annihilation.

Note that there is an additional GRG observation by Eack et al. (1996a) that we did not consider in this work. It reported a GRG detected at 4 km altitude with an increase above background of about a factor 100. This was completely out-of-scope of what our model was able to produce in the tested potential range (−220 to +220 MV). It would have required extremely high potential, largely above the RREA threshold.

Using GEANT4, we calculated effective areas, or equivalently detection efficiencies as function of energy, for photons, electrons and positrons; that is only what is needed, as we will work with relative increases over background only. In this study, the geometry of the detectors was simulated using GEANT4, which enabled us to consider the full range of physics related to electro-magnetic particles, including Compton scattering, pair production, photo-electric absorption for photons, scatterings and Bremsstrahlung for electrons and positrons, and annihilation for positrons. The used instrumental responses for the five detectors, in the form of effective area curves, for vertically incident photons, electrons and positrons, are provided in the data availability statement (Sarria, 2022b). For simplicity, we did not consider responses as a function of the incoming angle, and assumed always vertical. It is worth mentioning that, in most cases, the majority of particles detected are photons. This is due to their ability to travel longer distances and/or penetrate more easily through materials such as the structure of the plane or detector shielding.

The response functions are used together with the simulated photons, electron and positron spectra resulting from the (described above) GRG simulation library, and a relative increase of detector counts with respect to background (noted F_{inc}) is determined. If there is no increase over background, $F_{\text{inc}} = 1$. The values of F_{inc} were calculated at each altitude-potential grid point (see previous section), and values in-between were obtained using bi-linear interpolation on $\log(F_{\text{inc}})$.

4.2. Results

Figures 4–7 summarizes our final simulation results for glow observations by Eack 1996 and 2000 (Eack et al., 1996b, 2000), ADELE (Kelley et al., 2015), ILDAS (Kochkin et al., 2017). The case of ALOFT is shown

Figure 3. Example of content of the GRG simulation library. The E-field center altitude is set to 14 km, full length (in altitude) is 2 km and the all the particles are recorded at 15 km altitude. (a) Increase factors of photons electrons and positrons as function of the applied potential. (b, c) Photon energy spectrum for all the potentials. (d, e) Electron energy spectrum for all the potentials. (f, g) Positron energy spectrum for all the potentials. For the spectra, the y-units are arbitrary, but the relative scales between all the spectra and particle types are respected. For potentials close to 0 MV, the spectra are consistent with the ones given by PARMA/EXPACS (Sato et al., 2008). When the potential are increased from 0 to 220 MV, the energy spectra evolves toward a characteristic RREA spectrum that is a power law with an exponential cut-off (E_{th} is for 126 MV for $H_E = 14$ km). When the potential evolves in the negative, RREA is produced downwards and only the back-scattered RREA is detected. In addition, the positrons are accelerated toward the detection altitude and show a harder energy spectrum.

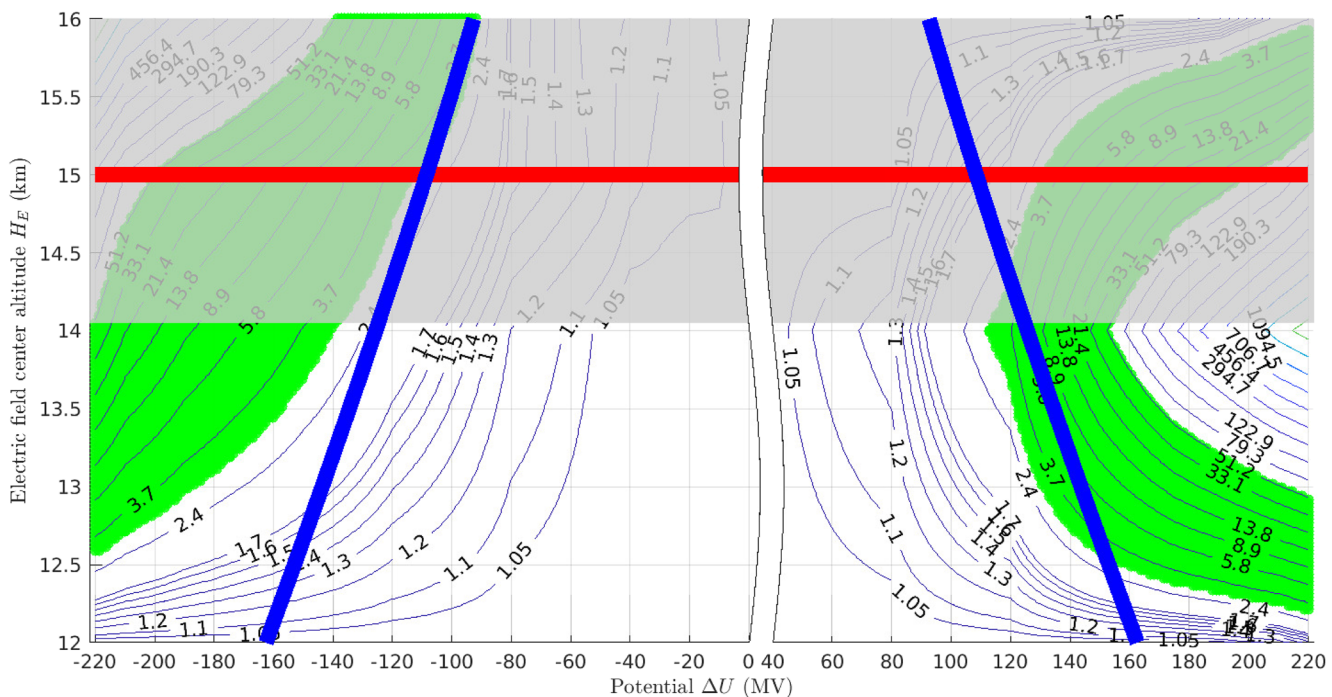


Figure 4. Level curves of detector counts multiplication factors (F_{inc}) as function of E-field center altitude (H_E) and applied potential for results of the Eack 1996 campaign (Eack et al., 1996b). The extension of the electric field region (ΔH_E) is always 2 km. The red line is the detection altitude of the given observation. The blue curves indicate the RREA threshold F_{th} . The green area indicates where the observed flux increase is compatible with the observation. The gray area indicates a part of the parameter space that can be excluded.

in Østgaard et al. (2019), Figure 9, that was obtained with an earlier version of the same models used here (GRG production/propagation, and detector response). Figures 4–7 show level curve plots of F_{inc} , as function of the center-altitude of the E-field region (H_E), and the applied potential (ΔU). As indicated previously, the E-field region has a 2 km full length (ΔH_E) for any center-altitude. The red line is the detection altitude of the given observation (where the response of the given instrument is applied). The blue curves indicate the RREA threshold E_{th} that is function of H_E and ΔU : a large increase of F_{inc} is expected above it. The green area is where the flux increase is within the ranges of values are given in Table 1. The gray area represents the portion of the parameter space that is excluded because of the location of the cloud top, which was estimated approximately for each event.

Figure 4 shows the simulation result corresponding to conditions of the observations presented in Eack et al. (1996b). For this observation at 15 km altitude, the balloon was above the thunderstorm, therefore compatible configurations for higher altitudes can be ignored. We define “compatible” as a simulated flux increase within the range of observed flux increases. Our simulation shows that both positive and negative potentials above $|E_{\text{th}}|$ can explain the observed count increase above background, and there are compatible configurations for any H_E above 12.5 km, with the appropriate potential. For an electric field region closer to the detection altitude, it is easier to have a large F_{inc} . The lowest required configuration to have F_{inc} of 3 is an electric field located between 13 and 15 km altitude ($H_E = 14$ km) with a potential of about +120 MV inside, that is slightly below E_{th} . This configuration is the most favorable for glow production, as the electrons get a 2 km long acceleration region and are recorded exactly at the end of it. In order to produce an increase that has the same magnitude as the strongest glow observed in the paper ($F_{\text{inc}} \approx 50$), a potential of 160 MV is required, that is 1.3 times the RREA threshold (E_{th}) at 14 km altitude, and increases to 220 MV (1.6 E_{th}) just 1 km below. Eack et al. (1996b) also reports a measurement of the electric field magnitude, that shows an electric field always far below E_{th} , and mostly located between 2 and 11 km altitude, that is out of range of the E-field location required by our simulations.

Figure 5 shows the simulation result concerning the observations presented in Eack et al. (2000). For this case, the balloon is at 14 km altitude, most likely above the thundercloud region (and electric field) therefore the compatible configurations for altitudes above it can be ignored. H_E located between 10.5 and 14 km altitude can produce a compatible F_{inc} between 1.6 and 3, as observed. The minimal required ΔU is also 120 MV for H_E at the

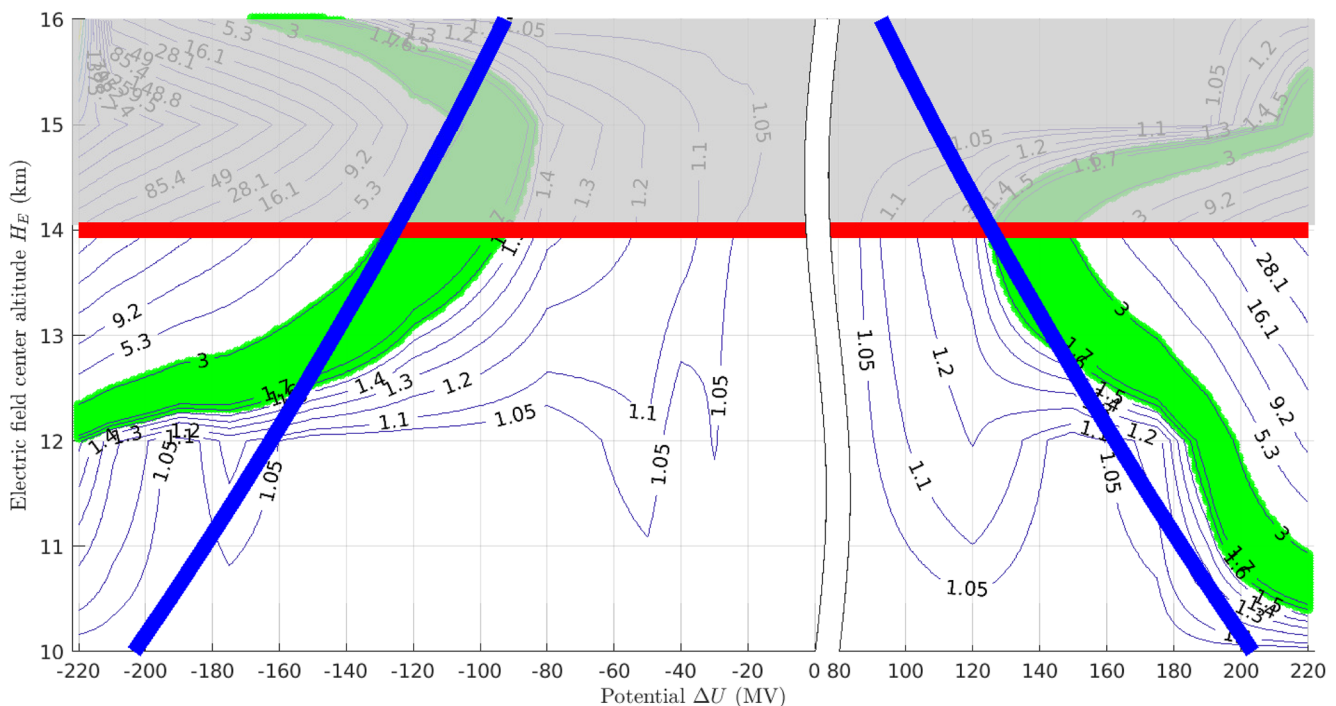


Figure 5. Level curves of detector counts multiplication factors (F_{inc}) as function of E-field center altitude H_E (km) and applied potential for results of the Eack 2000 campaign (Eack et al., 2000). The extension of the electric field region (ΔH_E) is always 2 km. The red line is the detection altitude of the given observation. The blue curves indicate the RREA threshold E_{th} . The green area indicates where F_{inc} is compatible with the observation. The gray area indicates a part of the parameter space that can be excluded.

same altitude level as the detector, and a potential up to 200 MV is required for $H_E = 11$ km. For lower altitudes, very large un-tested potential are required ($|\Delta U| > 220$ MV). In this case, the MOS mechanism (E-field below E_{th}) can explain all the observed fluxes for negative potentials, assuming the balloon is inside, or very close to the E-field region. The largest flux increase can be explained for ΔU corresponding to 1.3 times the RREA threshold (E_{th}) at a center altitude of 12 km. Both Eack et al. (2000) and Eack et al. (1996b) observations were made above continental US (Kansas, Oklahoma), and therefore E-field regions above 14 km altitude are unlikely (see Figure 5 in Eack and Beasley (2015)).

Figure 6 shows the simulation result concerning the observations by the ADELE instrument presented in Kelley et al. (2015) by the plastic detectors on-board a Gulfstream-V aircraft. In this case the observed glows, with F_{inc} between 1.2 and 10 can also be explained with a large interval of H_E between 10 and 16 km, above, below or at the level of the aircraft. As for the previous cases, compatible F_{inc} can be obtained when the E-field is close to E_{th} . For F_{inc} to increase from 1.2 to 10, a raise of 80% of ΔU is necessary, meaning an electric field significantly above E_{th} . The reported observations where also obtained above continental US (Colorado and Florida) and radar data indicating a cloud top close to 14 km altitude is mentioned for one even.

Figure 7 shows the simulation result concerning the observations by the ILDAS LaBr₃-based X/gamma-ray detector located inside an A340 aircraft, presented in Kochkin et al. (2017). The article indicates that the cloud top height is close to 15 km altitude, so values above this can be ignored. In this case, we see that compatible values of F_{inc} can be only produced using negative potentials. With negative potentials, the electrons are accelerated downwards and therefore the E-field region (and its center altitude H_E) should be above the aircraft (located at about 12 km altitude). Compared to previous observations, the minimal potential condition to reproduce the observed F_{inc} of 3 is to have a potential of <-170 MV at 14 km altitude, that is 25% above the RREA threshold (E_{th}). To reproduce the maximum observed F_{inc} of about 20, a potential <-210 MV is required, that is very large ($1.75E_{\text{th}}$).

The case of ALOFT is shown in Østgaard et al. (2019), that was obtained using an earlier version of the models presented here (glow generation, propagation and instrument response). This campaign contained BGO detectors inside the pod of a ER-2 aircraft flying at 20 km altitude. The figure shows simulation results of a GRG detected

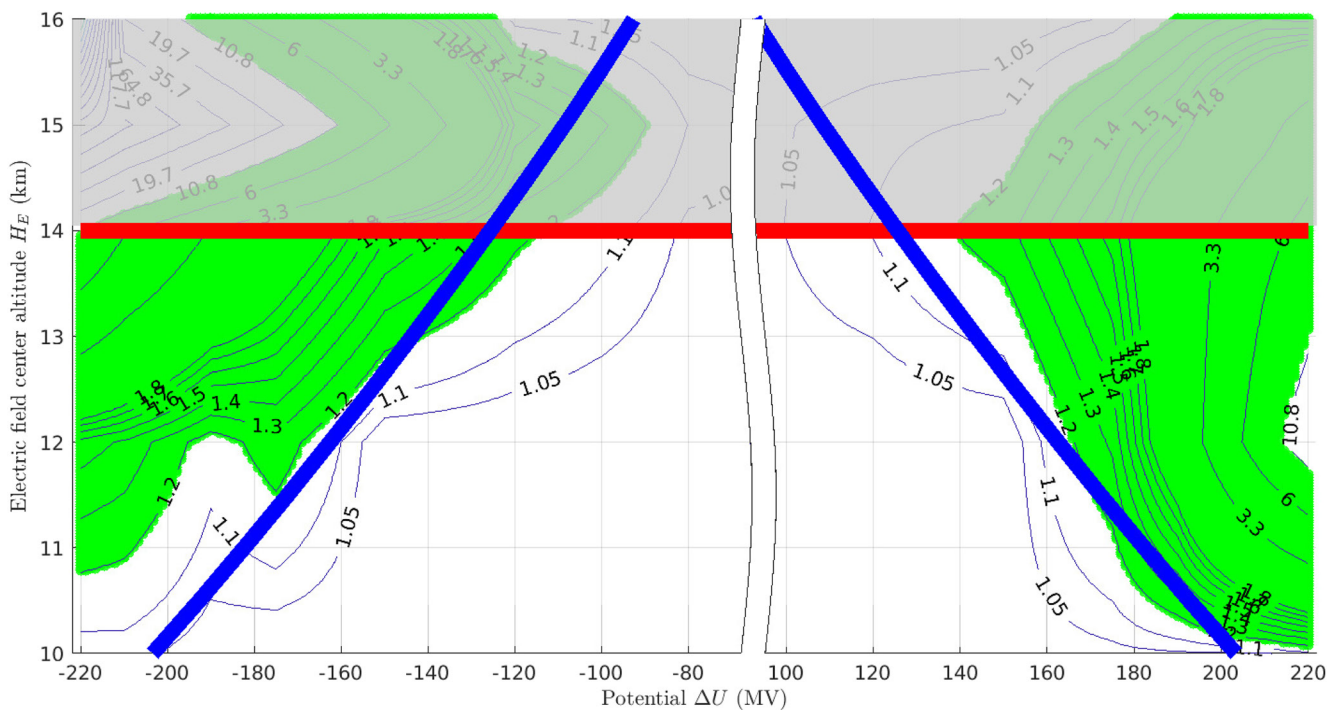


Figure 6. Level curves of detector counts multiplication factors (F_{inc}) as function of E-field center altitude H_E (km) and applied potential for results of the ADELE campaign (Kelley et al., 2015). The extension of the electric field region (ΔH_E) is always 2 km. The red line is the detection altitude of the given observation. The blue curves indicate the RREA threshold E_{th} . The green area indicates where F_{inc} is compatible with the observation. The gray area indicates a part of the parameter space that can be excluded.

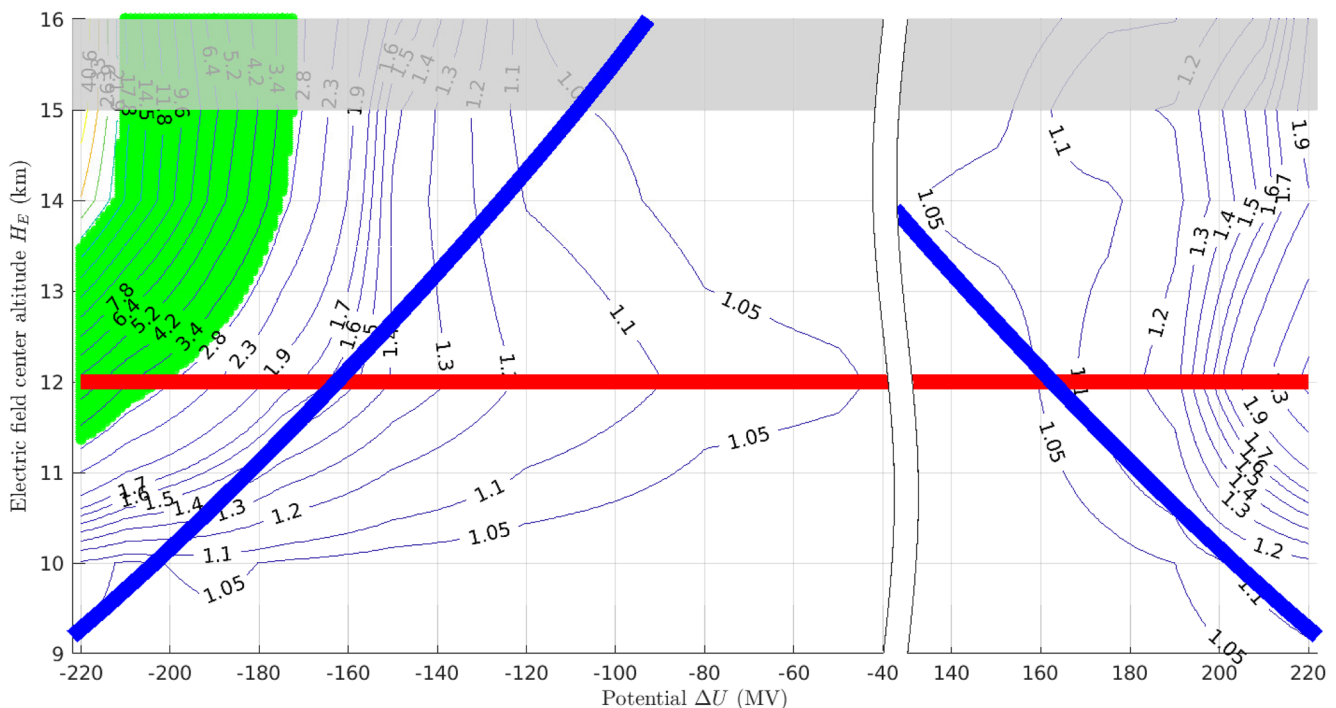


Figure 7. Level curves of detector counts multiplication factors (F_{inc}) as function of E-field center altitude H_E (km) and applied potential for results of the ILDAS campaign (Kochkin et al., 2017). The extension of the electric field region (ΔH_E) is always 2 km. The red line is the detection altitude of the given observation. The blue curves indicate the RREA threshold E_{th} . The green area indicates where F_{inc} is compatible with the observation. The gray area indicates a part of the parameter space that can be excluded.

at 20 km altitude with a source H_E between 9 and 12 km altitude. In this case ΔH_E was also 2 km. It was showed that only negative ΔU (electrons accelerated upwards) gave possible solutions as positive ΔU could lead to a background increase larger than the simulation noise level. Note that we inverted the polarity definition here, compared to Østgaard et al. (2019)). Possible solutions have H_E between 9 and 12 km due to constraints coming from other measurements (see description in Østgaard et al. (2019)), and higher altitudes were not tested as they are incompatible with the measured cloud top. In this altitude range, it was shown that the required potential to produce a glow with a F_{inc} between 1.1 and 1.45 is about 20%–25% above the RREA threshold. This study also included spectral analysis, but the biggest constraint on H_E and ΔU was actually obtained from F_{inc} only, as compatible energy spectra were contained inside a fairly large parameter area.

5. Discussion

In the previous section, we showed that some glow observations could be explained by electric-fields only in the MOS regime, while some other observations require E to be at least at the level of the RREA threshold E_{th} . The latter corresponds to large electric field magnitude, that were never observed, to our knowledge. Eack et al. (1996b) could measure the electric field magnitude when the balloon was moving upwards inside, or around the thunderstorm. The on-board E-field meter measured an electric field of about 50 kV/m at 9 km altitude (see Figure 1 of Eack et al. (1996b)), that corresponds to a potential of 50 MV in our case (assuming a total E-field length of 2 km), that is about 44% of the RREA threshold. It should be noted that the measurement was taken at a specific point and at a particular altitude as the balloon was climbing. According to Eack and Beasley (2015), a simple model (as outlined in appendix B of the same publication) suggests that to account for the maximum E-field values observed at the balloon's level, electric fields slightly above the Break-Even field of 216 kV/m (at sea level), or 0.76 E_{th} would be required. It is possible that regions within the cloud may have larger electric fields, despite the lack of current evidence.

Our Monte Carlo model assumes that the detector is always positioned horizontally (i.e., in the X-Y plane) in the center of the electric field region, with varying altitude. For real glow events, it is generally assumed that the strength of the electric fields reaches a peak at a specific point, and then gradually decreases as one moves away from that point. Similarly, it is also assumed that the electron and gamma-ray fluxes will be at their highest at this peak electric-field point, and will gradually decrease as one moves away from it. Observations are not always made at the peak point, which means that events that have been concluded to be produced by the MOS regime may in fact be produced by the RREA regime, as there may be a stronger flux point than the one being observed. But than does not exclude that at least some, relatively weak, glow events can be produced by the MOS mechanism alone without need of RREA.

Both Eack et al. (2000) and Eack et al. (1996b) observations were made above continental US (Kansas, Oklahoma), and therefore E-field regions above 14 km altitude are highly unlikely. The highest possible E-field region could be between the upper positive charge region and a negative screening layer; or inverted for an anomalous charge system. In Østgaard et al. (2019), the reported glow observation was also made over continental US (Colorado) the upper cloud layer was reported to be at about 13 km altitude by the on-board Cloud Physics Lidar instrument. Therefore, for Eack et al. (2000) and Eack et al. (1996b) observations, scenarios with H_E around 12 km and E-fields above the RREA threshold are the most likely.

In Østgaard et al. (2019), extensive electric field and lightning activity measurement from ground and front the airplane were available. It was shown that the cloud polarity is most probably anomalous (positive), that means a large-scale electric field accelerating electrons downwards, that seems incompatible with the simulated GRG production scenario inside the cloud (as the detector was located above the cloud at 20 km altitude). We see two possible solutions to this issue: 1. even if the main thunderstorm structure is inverted (anomalous), the whole structure could be more complex and have somewhere a sub-charge structure with the correct polarity and a strong enough potential difference. 2. Østgaard et al. (2019) presents an alternative glow production scenario where the glow is produced by a large-scale electric field between the cloud top and the ionosphere. The problem with this scenario is that the electric field measurements from the onboard instrument did not report a strong enough E-field.

As written in the previous section, for the ADELE and ILDAS observations, large potential values of 1.75 E_{th} to 1.8 E_{th} are necessary to explain largest F_{inc} observed. Such values are quite challenging to explain for real

thunderstorm conditions, as it is not clear if such high potential can be reached before it dropping due to the movement of charges and ions. In addition, as already mentioned in Section 4, there is an additional GRG observation by Eack et al. (1996a) that we were not able to reproduce in this work. The glow was detected at 4 km altitude with an increase above background of about a factor 100. This is completely outside of what our model is able to produce as it probably requires extremely high potential, largely above the RREA threshold that we could not test, due to limitations of our simulation code in its current version. This case would be in the simulation state (iii), as described in Section 2. In this state, the relativistic feedback dominates the contribution to F_{inc} , and our simulation would require a more sophisticated management of a time step and limit in order to work properly. As discussed above, it is important to stress that the existence, in real life, of such high potential conditions (i.e., larger than the RREA threshold) is questionable, but remains an open question. For a discussion of maximum possible E-fields in thunderstorms, see Dwyer (2003). For a review of measurements see Stolzenburg and Marshall (2008), that always reports the E-fields at the edge or below the RREA threshold E_{th} .

For the cases requiring potentials more than 2 times the RREA threshold, another production mechanism could be responsible for the GRG production. It is possible that the mechanism presented here, purely based on thunderstorms' E-fields affecting the cosmic-ray background, can explain all the high altitude GRG observations (i.e., above 10 km altitude); but lower altitude glow, like in Eack et al. (1996a) at 4 km altitude, and some ground observations, may require another mechanism. This mechanism could be based on the afterglow of X/gamma-ray produced by radioactive isotopes disintegration (Babich, 2017; Bowers et al., 2017; Enoto et al., 2017; Rutjes et al., 2017; Wada et al., 2020); where the isotopes could be a consequence of a Terrestrial Gamma-ray Flash. In this scenario, glow durations of several tens of minutes were shown possible according to simulations by Diniz et al. (2021), using RREA seeding from β^+ decay particles. This involves that the observation from Eack et al. (1996a) at 4 km altitude could have been preceded by a TGF, that was not reported (while the opposite, a TGF produced at the termination/end of a GRG, was reported in Wada et al. (2019)).

This work did not include full spectral analysis, that could potentially reduce the range of compatible parameters between the model and observations presented above. An extensive spectral analysis of the ALOFT glow observation was performed in Østgaard et al. (2019) by essentially the same team as the present paper. A spectral analysis of the ADELE events was provided by Kelley et al. (2015). The observation by Eack et al. (1996b); Eack et al. (2000) are quite limited in regards of spectral analysis since they have only three energy bins with a maximum energy of 300 keV. To some extend, Eack and Beasley (2015) used a form of spectral analysis since they considered the three energy bins in their modeling to calculate the attenuation of the x-ray flux from the source to the detector (see Appendix A of Eack and Beasley (2015)). To date, no spectral analysis has been conducted on the ILDAS (non-positron) glow events (note that there was some spectral analysis on the ILDAS glow-positron event presented in Kochkin et al. (2018)). Spectral analysis is a complex task that should be done on an event-by-event basis.

6. Conclusions and Future Work

We presented a general Monte-Carlo GEANT4-based model of Gamma-ray Glow (GRG) production. This model was compared to another, completely independent, model from Zhou et al. (2016) relying on another Monte-Carlo framework and small differences were observed. By running our model, we build an extensive simulation library made available to the community (see the Open Research section). This library was used, together with several instrumental responses, to simulate (reproduce) five previous gamma-ray glow airborne observations. These observations are from five campaigns: balloons from Eack et al. (1996b), Eack et al. (2000); and aircrafts from ADELE (Kelley et al., 2015), ILDAS (Kochkin et al., 2017), and ALOFT (Østgaard et al., 2019).

We confirmed that fluxes of cosmic-ray secondary photons, electrons and positrons at a given altitude can be multiplied by several tens of percent to orders of magnitude due to thunderstorms' electric fields (if available potential differences are large enough), and therefore explain the GRG observations mentioned above. We showed that some GRG could be explained purely by the MOS process, while E-fields significantly larger than E_{th} are required to explain the strongest ones. Some of the observations also came with partial electric field measurements, that reported measurements always much lower than the RREA threshold. These measurements were sparse, and there is no guarantee that they measured the region of the thundercloud with the highest E-fields, where the GRGs are produced. This study shows evidence that there must be E-fields with magnitude equal or larger than E_{th} inside thunderstorms. To find them, more observations are required, possibly with an array of

several balloons and/or aircraft, and ground electric field and radio measurements, in order to get a complete picture of a thundercloud system producing a GRG.

In the literature, two quite different GRG observations were reported, described as positron events, showing glows with a strong enhancement of the 511 keV line (Dwyer et al., 2015; Kochkin et al., 2018). It is possible to investigate these two cases using the same modeling strategy as presented here. However they will require a deeper investigation by looking closely at the recorded energy spectra (after applying instrumental response) for an excess of the 511 keV annihilation line. Thankfully, both ADELE and ILDAS could measure spectra with several energy bins. This will be the subject of a future work.

In this work, we focused on airborne observations, but many GRGs were observed from ground (see introduction). Our model could be used in order to try to reproduce and explain these observations as well. Even if some measurements are at sea level (e.g., Wada et al., 2019), some are also from mountain altitudes. The provided simulation library uses a ground at sea level, and therefore would not be able to be used for mountain observations (e.g., Chilingarian et al., 2010; Tsuchiya et al., 2007) as it is, and would require a more specific simulation set-up (including back scattering from particles hitting the ground). At low altitudes, the background radiation can be composed of non-cosmic sources, such as natural radioactivity from ground (mountains) and radon, which are not taken into account in the current model.

Data Availability Statement

The model presented in Section 2 is available in the following repository: <https://doi.org/10.5281/zenodo.7129586> (Sarria, 2022a). There is no specific documentation, so we suggest the reader to read the documentations of GEANT4 and PARMA, and to contact David Sarria (david.sarria@uib.no) for more information. Note that the code uses the PARMA fortran code that is available here: <https://phits.jaea.go.jp/expacs/>, with the associated documentation.

The glow simulation library is provided in the following repository: <https://doi.org/10.5281/zenodo.7129650> (Sarria, 2022c), and comes with documentation in order to be useable by other researchers.

All the data directly presented in this article, together with the used instrumental responses, can be obtained in the following repository: <https://doi.org/10.5281/zenodo.7129672> (Sarria, 2022b).

Acknowledgments

We thank D.M. Smith for providing access to the ADELE mass model and for discussions and help on the instrument simulation results. This work was supported by the European Research Council under the European Union's Seventh Framework Program (FP7/2007–2013)/ERC grant agreement n. 320839 and the Research Council of Norway under contracts 208028/F50, 223252/F50 (CoE) and NFR 325582. The simulations were performed on resources provided by UNINETT Sigma2—the National Infrastructure for High Performance Computing and Data Storage in Norway, under project no. NN9526K. The authors thank the International Space Science Institute, Bern, Switzerland, for providing financial support and meeting facilities in the frame of the International Team no. 471: Understanding the Properties of the Terrestrial Gamma-Ray Flash Population. We would like to thank the three anonymous reviewers for their constructive questions and comments, which helped improve the quality of this work.

References

- Agostinelli, S., Allison, J., Amako, K., Apostolakis, J., Araujo, H., Arce, P., et al. (2003). GEANT4—A simulation toolkit. *Nuclear Instruments and Methods in Physics Research*, 506(3), 250–303. [https://doi.org/10.1016/S0168-9002\(03\)01368-8](https://doi.org/10.1016/S0168-9002(03)01368-8)
- Allison, J., Amako, K., Apostolakis, J., Araujo, H., Dubois, P. A., Asai, M., et al. (2006). Geant4 developments and applications. *IEEE Transactions on Nuclear Science*, 53(1), 270–278. <https://doi.org/10.1109/TNS.2006.869826>
- Babich, L. P. (2003). *High-energy phenomena in electric discharges in dense gases: Theory, experiment, and natural phenomena*. Futurepast Incorporated.
- Babich, L. P. (2017). Radiocarbon production by thunderstorms. *Geophysical Research Letters*, 44(21), 11191–11200. <https://doi.org/10.1002/2017GL075131>
- Bartoli, B., Bernardini, P., Bi, X. J., Cao, Z., Catalanotti, S., Chen, S., et al. (2018). Observation of the thunderstorm-related ground cosmic ray flux variations by argo-ybj. *Physical Review D*, 97(4), 042001. <https://doi.org/10.1103/PhysRevD.97.042001>
- Bowers, G. S., Smith, D. M., Martinez-McKinney, G., Kamogawa, M., Cummer, S., Dwyer, J., et al. (2017). Gamma-ray signatures of neutrons from a terrestrial gamma-ray flash. *Geophysical Research Letters*, 44(19), 10063–10070. <https://doi.org/10.1002/2017GL075071>
- Brunetti, M., Cecchini, S., Galli, M., Giovannini, G., & Pagliarin, A. (2000). Gamma-ray bursts of atmospheric origin in the MeV energy range. *Geophysical Research Letters*, 27(11), 1599–1602. <https://doi.org/10.1029/2000gl003750>
- Chanrion, O., Bonaventura, Z., Bourdon, A., & Neubert, T. (2016). Influence of the angular scattering of electrons on the runaway threshold in air. *Plasma Physics and Controlled Fusion*, 58(4), 044001. <https://doi.org/10.1088/0741-3335/58/4/044001>
- Chilingarian, A., Bostanjyan, N., & Vanyan, L. (2012). Neutron bursts associated with thunderstorms. *Physical Review D*, 85(8), 085017. <https://doi.org/10.1103/physrevd.85.085017>
- Chilingarian, A., Daryan, A., Arakelyan, K., Hovhannisan, A., Mailyan, B., Melkumyan, L., et al. (2010). Ground-based observations of thunderstorm-correlated fluxes of high-energy electrons, gamma rays, and neutrons. *Physical Review D*, 82(4), 043009. <https://doi.org/10.1103/physrevd.82.043009>
- Chilingarian, A., Vanyan, L., & Mailyan, B. (2013). Observation of thunderstorm ground enhancements with intense fluxes of high-energy electrons. *Astroparticle Physics*, 48, 1–7. <https://doi.org/10.1016/j.astropartphys.2013.06.006>
- Chubenko, A., Antonova, V., Kryukov, S. Y., Piskal, V., Ptitsyn, M., Shepetov, A., et al. (2000). Intensive x-ray emission bursts during thunderstorms. *Physics Letters A*, 275(1), 90–100. [https://doi.org/10.1016/S0375-9601\(00\)00502-8](https://doi.org/10.1016/S0375-9601(00)00502-8)
- Diniz, G. S., Ferreira, I. S., Wada, Y., & Enoto, T. (2021). Generation possibility of gamma-ray glows induced by photonuclear reactions. *Journal of Geophysical Research: Atmospheres*, 126(3), e2020JD034101. <https://doi.org/10.1029/2020JD034101>
- Dwyer, J. R. (2003). A fundamental limit on electric fields in air. *Geophysical Research Letters*, 30(20), 2055. <https://doi.org/10.1029/2003GL017781>
- Dwyer, J. R. (2012). The relativistic feedback discharge model of terrestrial gamma ray flashes. *Journal of Geophysical Research*, 117(A2), A02308. <https://doi.org/10.1029/2011JA017160>

- Dwyer, J. R., Smith, D. M., & Cummer, S. A. (2012). High-energy atmospheric physics: Terrestrial gamma-ray flashes and related phenomena. *Space Science Reviews*, 173(1–4), 133–196. <https://doi.org/10.1007/s11214-012-9894-0>
- Dwyer, J. R., Smith, D. M., Hazelton, B. J., Grefenstette, B. W., Kelley, N. A., Lowell, A. W., et al. (2015). Positron clouds within thunderstorms. *Journal of Plasma Physics*, 81(04), 475810405. <https://doi.org/10.1017/s0022377815000549>
- Eack, K. B. (1996). Balloon-borne x-ray spectrometer for detection of x rays produced by thunderstorms. *Review of Scientific Instruments*, 67(5), 2005–2009. <https://doi.org/10.1063/1.1146959>
- Eack, K. B., & Beasley, W. H. (2015). Long-duration x-ray emissions observed in thunderstorms. *Journal of Geophysical Research: Atmospheres*, 120(14), 6887–6897. <https://doi.org/10.1002/2015JD023262>
- Eack, K. B., Beasley, W. H., Rust, W. D., Marshall, T. C., & Stolzenburg, M. (1996a). Initial results from simultaneous observation of x-rays and electric fields in a thunderstorm. *Journal of Geophysical Research*, 101(D23), 29637–29640. <https://doi.org/10.1029/96jd01705>
- Eack, K. B., Beasley, W. H., Rust, W. D., Marshall, T. C., & Stolzenburg, M. (1996b). X-ray pulses observed above a mesoscale convective system. *Geophysical Research Letters*, 23(21), 2915–2918. <https://doi.org/10.1029/96gl02570>
- Eack, K. B., Suszynsky, D. M., Beasley, W. H., Roussel-Dupre, R., & Symbalisty, E. (2000). Gamma-ray emissions observed in a thunderstorm anvil. *Geophysical Research Letters*, 27(2), 185–188. <https://doi.org/10.1029/1999gl010849>
- Enoto, T., Wada, Y., Nakazawa, K., Yuasa, T., Okuda, K., et al. (2017). Photonuclear reactions triggered by lightning discharge. *Nature*, 551(481), 481–484. <https://doi.org/10.1038/nature24630>
- Gurevich, A., Antonova, V., Chubenko, A., Karashtin, A., Mitko, G., Ptitsyn, M., et al. (2012). Strong flux of low-energy neutrons produced by thunderstorms. *Physical Review Letters*, 108(12), 125001. <https://doi.org/10.1103/physrevlett.108.125001>
- Gurevich, A., Milikh, G., & Roussel-Dupre, R. (1992). Runaway electron mechanism of air breakdown and preconditioning during a thunderstorm. *Physics Letters A*, 165(5–6), 463–468. [https://doi.org/10.1016/0375-9601\(92\)90348-p](https://doi.org/10.1016/0375-9601(92)90348-p)
- Kelley, N. A., Smith, D. M., Dwyer, J. R., Splitter, M., Lazarus, S., Martinez-McKinney, F., et al. (2015). Relativistic electron avalanches as a thunderstorm discharge competing with lightning. *Nature Communications*, 6(1), 7845. <https://doi.org/10.1038/ncomms8845>
- Kochkin, P., Sarria, D., Skeie, C., van Deursen, A. P. J., de Boer, A. I., Bardet, M., et al. (2018). In-flight observation of positron annihilation by ildas. *Journal of Geophysical Research: Atmospheres*, 123(15), 8074–8090. <https://doi.org/10.1029/2018JD028337>
- Kochkin, P., van Deursen, A. P. J., Marisaldi, M., Ursi, A., de Boer, A. I., Bardet, M., et al. (2017). In-flight observation of gamma-ray glows by ildas. *Journal of Geophysical Research: Atmospheres*, 122(23), 12801–12811. <https://doi.org/10.1002/2017JD027405>
- Lehtinen, N. G. (2000). *Relativistic runaway electrons above thunderstorms* (Unpublished doctoral dissertation). Stanford University.
- McCarthy, M., & Parks, G. (1985). Further observations of x-rays inside thunderstorms. *Geophysical Research Letters*, 12(6), 393–396. <https://doi.org/10.1029/gl012i006p00393>
- Østgaard, N., Christian, H. J., Grove, J. E., Sarria, D., Mezentsev, A., Kochkin, P., et al. (2019). Gamma ray glow observations at 20-km altitude. *Journal of Geophysical Research: Atmospheres*, 124(13), 7236–7254. <https://doi.org/10.1029/2019JD030312>
- Parks, G., Mauk, B., Spiger, R., & Chin, J. (1981). X-ray enhancements detected during thunderstorm and lightning activities. *Geophysical Research Letters*, 8(11), 1176–1179. <https://doi.org/10.1029/gl008i011p01176>
- Rutjes, C., Diniz, G., Ferreira, I. S., & Ebert, U. (2017). TGF afterglows: A new radiation mechanism from thunderstorms. *Geophysical Research Letters*, 44(20), 10702–10712. <https://doi.org/10.1002/2017GL075552>
- Rutjes, C., Sarria, D., Broberg Skeltved, A., Luque, A., Diniz, G., Østgaard, N., & Ebert, U. (2016). Evaluation of Monte Carlo tools for high energy atmospheric physics. *Geoscientific Model Development*, 9(11), 3961–3974. <https://doi.org/10.5194/gmd-9-3961-2016>
- Sarria, D. (2022a). Cosmic ray thunderstorm GEANT4 [Software]. Zenodo. <https://doi.org/10.5281/zenodo.7129586>
- Sarria, D. (2022b). Data repository of the paper "library of simulated gamma-ray glows and application to previous airborne observations" by d. sarria et al [Dataset]. Zenodo. <https://doi.org/10.5281/zenodo.7129672>
- Sarria, D. (2022c). gamma-ray glow simulation library for the paper "library of simulated gamma-ray glows and application to previous airborne observations" by d. sarria et al [Dataset]. Zenodo. <https://doi.org/10.5281/zenodo.7129650>
- Sarria, D., Rutjes, C., Diniz, G., Luque, A., Ihaddadene, K. M. A., Dwyer, J. R., et al. (2018). Evaluation of Monte Carlo tools for high energy atmospheric physics II: Relativistic runaway electron avalanches. In *Geoscientific model development discussions*, 2018 (Vol. 1–30). <https://doi.org/10.5194/gmd-2018-119>
- Sato, T. (2016). Analytical model for estimating the zenith angle dependence of terrestrial cosmic ray fluxes. *PLoS One*, 11(8), 1–22. <https://doi.org/10.1371/journal.pone.0160390>
- Sato, T., Iwamoto, Y., Hashimoto, S., Ogawa, T., Furuta, T., ichiro Abe, S., et al. (2018). Features of particle and heavy ion transport code system (PHITS) version 3.02. *Journal of Nuclear Science and Technology*, 55(6), 684–690. <https://doi.org/10.1080/00223131.2017.1419890>
- Sato, T., Yasuda, H., Niita, K., Endo, A., & Silver, L. (2008). Development of PARMA: PHITS-based analytical radiation model in the atmosphere. *Radiation Research*, 170(2), 244–259. <https://doi.org/10.1667/RR1094.1>
- Skeltved, A. B., Østgaard, N., Carlson, B., Gjesteland, T., & Celestin, S. (2014). Modeling the relativistic runaway electron avalanche and the feedback mechanism with GEANT4. *Journal of Geophysical Research: Space Physics*, 119(11), 9174–9191. <https://doi.org/10.1002/2014JA020504>
- Smith, D. M., Bowers, G. S., Kamogawa, M., Wang, D., Ushio, T., Ortberg, J., et al. (2018). Characterizing upward lightning with and without a terrestrial gamma ray flash. *Journal of Geophysical Research: Atmospheres*, 123(20), 11321–11332. <https://doi.org/10.1029/2018JD029105>
- Stolzenburg, M., & Marshall, T. C. (2008). Charge structure and dynamics in thunderstorms. In F. Leblanc, K. L. Aplin, Y. Yair, R. G. Harrison, J. P. Lebreton, & M. Blanc (Eds.), *Planetary atmospheric electricity* (pp. 355–372). Springer. https://doi.org/10.1007/978-0-387-87664-1_23
- Torii, T., Sugita, T., Tanabe, S., Kimura, Y., Kamogawa, M., Yajima, K., & Yasuda, H. (2009). Gradual increase of energetic radiation associated with thunderstorm activity at the top of mt. Fuji. *Geophysical Research Letters*, 36(13), L13804. <https://doi.org/10.1029/2008gl037105>
- Torii, T., Takeishi, M., & Hosono, T. (2002). Observation of gamma-ray dose increase associated with winter thunderstorm and lightning activity. *Journal of Geophysical Research*, 107(D17), ACL2-1–ACL2-13. <https://doi.org/10.1029/2001jd000938>
- Tsuchiya, H., Enoto, T., Yamada, S., Yuasa, T., Kawaharada, M., Kitaguchi, T., et al. (2007). Detection of high-energy gamma rays from winter thunderclouds. *Physical Review Letters*, 99(16), 165002. <https://doi.org/10.1103/physrevlett.99.165002>
- Tsuchiya, H., Hibino, K., Kawata, K., Hotta, N., Tateyama, N., Ohnishi, M., et al. (2012). Observation of thundercloud-related gamma rays and neutrons in Tibet. *Physical Review D*, 85(9), 092006. <https://doi.org/10.1103/physrevd.85.092006>
- Wada, Y., Bowers, G. S., Enoto, T., Kamogawa, M., Nakamura, Y., Morimoto, T., et al. (2018). Termination of electron acceleration in thundercloud by intracloud/intercloud discharge. *Geophysical Research Letters*, 45(11), 5700–5707. <https://doi.org/10.1029/2018GL077784>
- Wada, Y., Enoto, T., Nakamura, Y., Furuta, Y., Yuasa, T., Nakazawa, K., et al. (2019). Gamma-ray glow preceding downward terrestrial gamma-ray flash. *Communications Physics*, 2(1), 67. <https://doi.org/10.1038/s42005-019-0168-y>
- Wada, Y., Enoto, T., Nakazawa, K., Odaka, H., Furuta, Y., & Tsuchiya, H. (2020). Photonuclear reactions in lightning: 1. Verification and modeling of reaction and propagation processes. *Journal of Geophysical Research: Atmospheres*, 125(20), e2020JD033193. <https://doi.org/10.1029/2020JD033193>

- Wada, Y., Matsumoto, T., Enoto, T., Nakazawa, K., Yuasa, T., Furuta, Y., et al. (2021). Catalog of gamma-ray glows during four winter seasons in Japan. *Physical Review Research*, 3(4), 043117. <https://doi.org/10.1103/PhysRevResearch.3.043117>
- Wilson, C. T. R. (1925). The acceleration of β -particles in strong electric fields such as those of thunderclouds. *Proceedings of the Cambridge Philosophical Society*, 22(4), 534–538. <https://doi.org/10.1017/S0305004100003236>
- Zhou, X., Wang, X., Huang, D., & Jia, H. (2016). Effect of near-earth thunderstorms electric field on the intensity of ground cosmic ray positrons/electrons in Tibet. *Astroparticle Physics*, 84, 107–114. <https://doi.org/10.1016/j.astropartphys.2016.08.004>